Old Dominion University

ODU Digital Commons

2021

Synoptic Mesoscale to Basin Scale Variability in Biological Productivity and Chlorophyll in the Kuroshio Extension Region

Sophie Clayton
Old Dominion University, sophie.clayton@noc.ac.uk

Hilary I. Palevsky
Boston College, palevsky@bc.edu

LuAnne Thompson
University of Washington, luanne@uw.edu

Paul D. Quay
University of Washington, pdquay@uw.edu

Follow this and additional works at: https://digitalcommons.odu.edu/oeas_fac_pubs

Part of the Oceanography Commons

Synoptic Mesoscale to Basin Scale Variability in Biological Productivity and Chlorophyll in the Kuroshio Extension Region

Sophie Clayton[1] [iD], **Hilary I. Palevsky[2]** [iD], **LuAnne Thompson[3]** [iD], **and Paul D. Quay[3]** [iD]

[1]Department of Ocean and Earth Sciences, Old Dominion University, Norfolk, VA, USA, [2]Department of Earth and Environmental Sciences, Boston College, Boston, MA, USA, [3]School of Oceanography, University of Washington, Seattle, WA, USA

Abstract The Kuroshio current separates from the Japanese coast to become the eastward flowing Kuroshio Extension (KE) characterized by a strong latitudinal density front, high levels of mesoscale (eddy) energy, and high chlorophyll *a* (Chl). While satellite measurements of Chl show evidence of the impact of mesoscale eddies on the standing stock of phytoplankton, there have been very limited synoptic, spatially resolved in situ estimates of productivity in this region. Here, we present underway measurements of oxygen/argon supersaturation ($\Delta O_2/Ar$), a tracer of net biological productivity, for the KE made in spring, summer, and early autumn. We find large seasonal differences in the relationships between $\Delta O_2/Ar$, Chl, and sea level anomaly (SLA), a proxy for local thermocline depth deviations driven by mesoscale eddies derived from satellite observations. We show that the KE is a pronounced hotspot of high $\Delta O_2/Ar$ in spring, but corresponding surface Chl values are low and have no correlation with $\Delta O_2/Ar$. In summer, there is a hotspot of productivity associated with the Oyashio front, where $\Delta O_2/Ar$ and Chl are strongly positively correlated. In autumn, $\Delta O_2/Ar$ and Chl are consistently low throughout the region and also positively correlated. By combining our analysis of the in situ $\Delta O_2/Ar$ data with complementary Argo, BGC-Argo, repeat hydrography, and SLA observations, we infer the combination of physical and biological controls that drive the observed distributions of $\Delta O_2/Ar$ and Chl. We find that the KE and Oyashio currents both act to supply nutrients laterally, fueling regions of high productivity in spring and summer, respectively.

Plain Language Summary Biological processes in the surface ocean play an important role in the ocean carbon cycle. Phytoplankton transform carbon dioxide into organic material, a portion of which then sinks into the deep ocean where it can be stored long term. This mechanism of carbon transfer from the surface to the deep ocean is known as the biological carbon pump. The processes that mediate the biological carbon pump can occur over short time and space scales. This is especially true in dynamic ocean systems such as western boundary currents like the Kuroshio Extension (KE), where there are local maxima in weekly to interannual variability in biogeochemical properties within the boundary current itself. Here we use novel continuous measurements made from ships of opportunity to explore the variability in productivity and chlorophyll and how they are connected to physical ocean dynamics. We show that the KE and Oyashio fronts are hotspots of productivity in spring and summer, respectively. However, this high productivity may not be well represented by chlorophyll *a*, a proxy for the standing stock of phytoplankton.

1. Introduction

The biological pump, the export of organic carbon from the surface to the deep ocean, plays a key role in the global carbon cycle (Giering & Humphreys, 2018; Volk & Hoffert, 1985). Inorganic carbon is converted to organic carbon by phytoplankton in the surface ocean through photosynthesis. A portion of this organic carbon is then exported from the surface and remineralized as it sinks through the water column, and is ultimately stored in the deep ocean with residence times of many months to centuries (DeVries et al., 2012). The processes that control the production, consumption, packaging, and export of organic carbon occur over relatively short time scales, from days to months, associated with biological processes, ecosystem dynamics, and the evolution of the surface mixed-layer and mesoscale motions (Bach et al., 2019; Buesseler
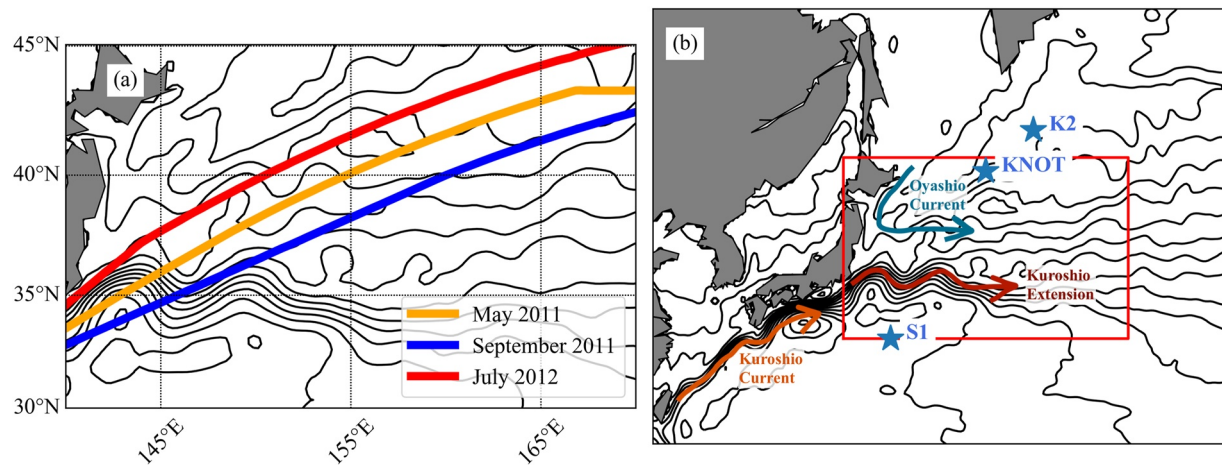
Figure 1. (a) Ship tracks for the three container ship cruises (May 2011, July 2012, and September 2011) shown over contours of the mean dynamic topography (MDT) for the KE region, as defined in Section 2. (b) Large scale circulation and MDT over the Northwest Pacific showing the major currents impacting the region. The KE sub-region targeted in this study and shown in panel (a) is indicated by the red box and the locations of long-term time-series sites S1, K2, and Station KNOT are indicated by blue stars.

et al., 2020; Ducklow et al., 2001). More specifically, the time scales that control the production and export of carbon from the surface ocean span the division rate of phytoplankton cells (1 day^{-1}; Ribalet et al., 2015), bloom events that last for weeks (Racault et al., 2012), and the seasonality of organic carbon production over the annual cycle in the mid and high latitudes (Haskell et al., 2020; Palevsky, Quay, Lockwood, et al., 2016). The spatial distribution of biogeochemical tracers in the surface ocean is also known to be very patchy, varying widely over scales as fine as (<1 km) (Mackas et al., 1985; Martin & Srokosz, 2002; van Gennip et al., 2016) up to basin scales (1,000 km). This temporal and spatial variability presents a challenge to observing and understanding the physical and biological drivers that control the production and export of organic carbon, particularly in highly dynamic ocean regions such as western boundary currents.

1.1. Productivity in the Kuroshio Extension Region

Western boundary current extensions are characterized by strong zonal currents and a strong density front. They are also characterized by mesoscale dynamics that have been hypothesized to be strong drivers of primary production (Mahadevan, 2015) and export (Honda et al., 2018). As a result of this multi-scale variability in time and space, western boundary current regions present a particular challenge to making observations that resolve key biogeochemical processes synoptically (Henson et al., 2016; Todd et al., 2019).

The Kuroshio Extension (KE) is the eastward extension of the Kuroshio western boundary current of the subtropical gyre in the North Pacific, turning eastward after separating off the coast of Japan. The seasonal cycle of primary productivity in this region is relatively well known from moored time-series studies, for example, Station S1 (30°N, 145°E) in the subtropical gyre, and Station K2 (47°N, 160°E) and the Kyodo North Pacific Ocean Time-Series (KNOT, 44°N, 155°E) in the subarctic gyre (see Figure 1b). Estimates of net primary production (NPP) rates obtained by ^{13}C incubations from these time series sites are very similar on an annual basis but the seasonal cycle depends on location. NPP is higher in the subarctic versus the subtropical gyre in summer and fall, and the reverse is true in the winter and spring (Imai et al., 2002; Matsumoto et al., 2016). Carbon budgets at these times series sites have shown a larger annual organic carbon flux to depth in the subtropical than the subarctic gyre, though the subarctic experiences a more pronounced seasonal cycle with greater net photosynthesis in summer counterbalanced by greater net remineralization in winter (Honda et al., 2017; Wakita et al., 2016). Although time series at individual locations have given insights into ocean biogeochemical processes, they do not fully describe the spatial variability found in the most dynamic ocean regions (Henson et al., 2016) where these pointwise measurements can alias spatial variability. Estimates of KE primary and net community production (NCP) rates based on data from regional transects differ from the seasonal and annual rates determined at individual time-series sites,

highlighting the importance of resolving spatially varying productivity rates in this region (Palevsky, Quay, Lockwood, et al., 2016).

The Kuroshio and KE have been shown to act as a large-scale subsurface nutrient stream, supporting large lateral transports of nutrients within the upper thermocline (Guo et al., 2012, 2013). The KE is effective in transporting nutrients in part because of its large volume transports. In addition, eddy scale motions can result in interleaving that creates anomalies of nutrients in the vertical and results in anomalously high subsurface nutrient concentrations compared to adjacent waters along the same isopycnals (Nagai & Clayton, 2017). The KE nutrient stream thus acts to increase the availability of nutrients in the euphotic zone, particularly within shoaling isopycnals associated with cyclonic eddies (negative sea level anomalies) that bring the nutricline closer to the surface. Adiabatic shoaling of the surface mixed layer can act to enhance productivity by uplifting isopycnals and the nutricline into the euphotic zone resulting in higher nutrient availability, rather than by mixing nutrients up into the surface mixed layer (McGillicuddy, 2016). Using satellite measured sea level anomalies (SLAs) and satellite estimates of chlorophyll a (referred to in this paper hereafter as Chl), Kouketsu et al. (2015) showed a negative correlation between SLA and Chl concentrations in the KE region, suggesting that higher Chl is associated with cyclonic eddies (negative SLA). They also showed seasonal differences in the strength of the correlations between SLA and Chl, suggesting seasonal dynamics in the coupling between mesoscale eddies and Chl. However, in situ observational evidence that supports the role of mesoscale dynamics in nutrient delivery is still limited (Clayton et al., 2014; Nagai & Clayton, 2017).

The temporal and spatial variability of the KE and its associated mesoscale eddy activity is driven by geostrophic processes that are along isopycnals: that is, their dynamics do not depend on mixing processes and flow is along isopycnal surfaces. Geostrophic mesoscale eddies can drive local shoaling/deepening of the mixed layer depth (MLD; and the nutricline). In addition, and coupling between mesoscale and submesoscales can enhance along-isopycnal vertical fluxes near-surface fronts (Ramachandran et al., 2014). The KE region is also subject to small-scale, localized regions of enhanced diabatic, cross-isopycnal, mixing, and turbulent dissipation. Microstructure profiles in the Kuroshio and KE frontal zones have shown high rates of turbulent dissipation in the thermocline and the base of the mixed layer (D'Asaro et al., 2011; Nagai et al., 2009), which could be an additional important driver of vertical nutrient fluxes, particularly to the north of the KE front (Kaneko et al., 2013). Consequently, the modulation of the MLD and the vertical supply of nutrients in the KE region is driven by a range of both along-isopycnal and cross-isopycnal (mixing) processes acting on a range of time and space scales. This likely will result in high spatial variability in productivity, which has not been resolved by existing in situ time-series studies, while the subsurface environment is not directly observed by satellite remote sensing.

1.2. Tracing Biological Productivity In Situ

Synoptic measurements of physical, chemical, and biological parameters made at appropriate scales are necessary to understand the balance of processes that control rates of productivity in the surface ocean. These types of measurements are also necessary to determine whether these processes are fully spatially resolved, or at least well parameterized, in large-scale climate models used to make predictions about changes in ocean biogeochemical processes, and their impact on the global carbon cycle. However, measuring productivity in situ can be challenging as traditional bottle methods for estimating productivity rates are labor-intensive and do not allow for a large number of estimates to be made either at high resolution or synoptically over large regions. Remotely sensed productivity estimates can be made over large areas, but do not resolve fine-scale variability, nor do they give information about the subsurface fields, and are subject to substantial uncertainty (Carr et al., 2006; Palevsky, Quay, & Nicholson, 2016). As a result, although it is well known that phytoplankton standing stocks (e.g., measured by chlorophyll fluorescence, cell counts, and particulate organic carbon) are extremely patchy in time and space (Mackas et al., 1985), little is known about the scales over which rates of productivity vary.

Non-incubation-based dissolved gas tracers have been used to derive synoptic, high-resolution estimates of net biological productivity. Measurements of the oxygen/argon (O_2/Ar) dissolved gas ratio in the surface mixed layer trace the balance between photosynthesis and respiration, where net autotrophic conditions contribute to biological oxygen supersaturation, and comparison to argon, a noble gas with similar physical

properties to oxygen, normalizes for physical drivers of oxygen supersaturation from bubble injection and temperature changes (Craig & Hayward, 2011; Emerson et al., 1991). The development of continuous underway methods to measure O_2/Ar (Cassar et al., 2009; Kaiser et al., 2005; Tortell, 2005) has enabled new fine spatial-scale measurements which have been widely applied in both coastal and open ocean regions (Castro-Morales et al., 2013; Estapa et al., 2015; Eveleth et al., 2017; Hamme et al., 2012; Izett et al., 2018; Kaiser et al., 2005; Lockwood et al., 2012; Manning et al., 2017; Palevsky et al., 2013; Rosengard et al., 2020; Stanley et al., 2010; Tortell et al., 2015, 2011; Ulfsbo et al., 2014). These data are frequently combined with an estimate of air-sea gas exchange to calculate a rate of air-sea biological oxygen flux (termed "bioflux" by Jonsson et al., 2013), which under steady-state conditions with negligible physical flux of oxygen in out of the mixed layer, is equivalent to mixed layer NCP (equivalent to gross primary production minus community respiration). In steady-state conditions with no transient change in the surface biomass concentration, NCP represents the rate of organic carbon export from the mixed layer.

Since the initial introduction of this method, important advances have been made in understanding potential biases that can complicate the interpretation of bioflux as NCP, particularly in dynamic physical environments strongly influenced by upwelling and entrainment such as in coastal regions (e.g., Haskell & Fleming, 2018; Izett et al., 2018; Jonsson et al., 2013; Teeter et al., 2018; Wang et al., 2020). Analysis with a high-resolution physical model has shown that these biases are most pronounced in coastal wind-driven upwelling systems with low oxygen waters underlying the surface mixed layer, but are much less important in offshore regions (Teeter et al., 2018). Previous analysis of the mixed layer O_2/Ar budget in the KE region of the North Pacific has shown that these biases are limited over large scales during the period from springtime restratification through fall (Palevsky, Quay, Lockwood, et al., 2016); however, potential biases in interpreting bioflux as NCP have not been tested at higher spatial resolution on synoptic scales in an eddy-resolving model in a western boundary current region analogous to the KE. This is a highly physically dynamic region, but as outlined above, unlike the coastal regions where strong biases have been shown due to upwelling and entrainment (e.g., Haskell & Fleming, 2018; Izett et al., 2018; Teeter et al., 2018; Wang et al., 2020), the shoaling/deepening of the surface mixed layer by fronts and eddies in western boundary current regions is primarily an adiabatic process that does not result in entrainment of waters into the surface mixed layer from below. This adiabatic driver of mixed layer shoaling/deepening will greatly limit the influence of the vertical physical supply term on the O_2/Ar budget despite the presence of vertical motions in the surface mixed layer. However, a few targeted studies of vertical microstructure have shown localized areas of high turbulent dissipation associated with the northern wall of the KE front (Kaneko et al., 2013), as well as south of the KE front (Nagai et al., 2012), which could drive diabatic transport across isopycnals.

We analyze underway $\Delta O_2/Ar$ as a tracer of net biological productivity spanning the Northwest Pacific, encompassing the KE region, from three different seasons: May 2011, September 2011, and July 2012. The continuous and simultaneous collection of underway measurements of dissolved gases, chlorophyll fluorescence, and physical ocean properties (e.g., temperature and salinity) allows us to examine the relationship between physical and biogeochemical tracers within these three high spatial resolution snapshots, with the measurements taken over about a week on each transect. The high temporal resolution of these continuous underway measurements also resolves variability from the mesoscale (∼10–100 km) to the basin scale (∼1,000 km). We use satellite SLA data to identify eddy activity along the cruise tracks and MLD estimates from Argo floats present in the region at the time of the cruises, allowing us to investigate the role of physical ocean dynamics in regional and seasonal variations in the relationship between $\Delta O_2/Ar$ and Chl. Additionally, the multiple transits giving high along-track resolution allow us to examine spatial variability as well as seasonal variations in $\Delta O_2/Ar$ and surface Chl and their relationship to each other, and the potential role of mesoscale eddies in driving enhanced net biological production in the surface mixed layer. We find large seasonal differences in the correlation between $\Delta O_2/Ar$ and surface Chl and show that they are decoupled in spring when $\Delta O_2/Ar$ is at its peak, but strongly coupled in summer and autumn. Finally, we propose hypotheses for the observed relationships between the distributions and variability of $\Delta O_2/Ar$ and Chl, suggesting a (de)coupling in the processes controlling these quantities in the larger KE region.

2. Data and Methods

In this study, we define the KE region of the North Pacific as the area bounded by 140°–170°E and 30°–45°N, following the definition in Palevsky, Quay, and Nicholson (2016) (the red box in Figure 1b). We combine data from several sources, described in detail below, including data collected underway from ships of opportunity (Figure 1a), remote sensing, repeat hydrographic surveys, and Biogeochemical-Argo floats (BGC-Argo). For reference, we have indicated the major currents impacting this region (Figure 1b): the Kuroshio, KE, and Oyashio. We will also refer to the KE front, which is the hydrographic front associated with the KE, which can be seen as a well-defined zonal feature with very closely spaced contours of sea surface height (mean dynamic topography [MDT] in Figure 1) at ~35°N.

2.1. Underway and Discrete Sampling for O_2/Ar and Chl

We continuously measured O_2/Ar dissolved gas ratios, temperature, salinity, and fluorescence from an underway seawater system, with an intake at 10 m, during basin-wide transects of the North Pacific on the M/V OOCL Tokyo (May and September 2011) and the M/V OOCL Tianjin (July 2012). These two ships are sister vessels with intakes at the same depth and identical setups for scientific sampling on board. For each transect, the container ships transited through the KE region defined above within about a week and crossed the KE front itself within a 24-h period, resulting in synoptic measurements. Temperature and salinity were measured using a Sea-Bird Electronics SBE45 thermosalinograph. Fluorescence was measured using a Seapoint Chlorophyll Fluorometer and calibrated to calculate underway chlorophyll-*a* concentrations for each cruise based on discrete samples collected from the underway seawater line every 6–8 h (including hours of daylight and darkness) and measured following standard methods on a Turner fluorometer (Strickland & Parsons, 1972).

Underway measurements of O_2/Ar dissolved gas ratios were made using continuous flow equilibrator inlet mass spectrometry (EIMS), following the method of Cassar et al. (2009). Water from the underway seawater system was pumped into an equilibrator cartridge (Membrana MicroModule G569, 0.75 in. × 1 in.), the headspace of which was delivered to a quadrupole mass spectrometer (Pfeiffer Prisma QMS) that measured individual ion currents at 1-s intervals. Ion current ratios for O_2/Ar are reported as the mean over a three-minute measurement period, chosen to match the e-folding response time for this EIMS setup. This yields a spatial resolution of ~2 km at the average ship speed of ~25 knots. Thus, both mesoscale and submesoscale features are resolved. For the September 2011 cruise, a Loess filter with a 30-min half-span was applied to remove high-frequency instrument noise, reducing the spatial resolution to ~40 km, giving a marginal sampling for mesoscale fields. This filter was not applied to the May 2011 or July 2012 cruises to preserve the spatial resolution of the data.

Seawater dissolved gas O_2/Ar ion current ratios from the shipboard mass spectrometer were calibrated by first correcting for instrument drift based on measurements of atmospheric O_2/Ar (a known standard) sampled for 30 min every 3 h, and second by calibrating to discrete seawater samples collected every 6–8 h by a ship rider from the science team and subsequently measured in a shore-based lab by IR-MS (Isotope Ratio Mass Spectrometer; see Palevsky, Quay, Lockwood, et al., 2016 for details of the discrete sample measurement procedures). The discrete sample calibration used a time-varying correction factor based on the weighted mean of the individual correction factors determined from the three nearest discrete samples. Uncertainty in the final corrected O_2/Ar EIMS measurements, determined based on comparison with the discrete IR-MS measurements, ranged from 0.4% to 1.0% across the three cruises.

2.2. Calculations of ΔO_2/Ar and Oxygen Bioflux

The biological oxygen saturation anomaly (ΔO_2/Ar) expressed as a percentage, calculated from measured O_2/Ar dissolved gas ratios is defined as:

$$\frac{\Delta O_2}{Ar} = \left[\frac{\left(\dfrac{O_2}{Ar} \right)_{meas}}{\left(\dfrac{O_2}{Ar} \right)_{eq}} - 1 \right] \times 100$$

The subscript "meas" represents the measured values and the subscript "eq" represents the temperature- and salinity-dependent concentrations of O_2 and Ar expected if the mixed layer were in equilibrium with the atmosphere, calculated from the solubility of both gases (Garcia & Gordon, 1992; Hamme & Emerson, 2004). In cases where the primary influences on dissolved gas concentrations in the mixed layer are biological effects and air-sea gas exchange, positive $\Delta O_2/Ar$ reflects biological oxygen supersaturation due to net autotrophic conditions, while negative $\Delta O_2/Ar$ reflects biological oxygen undersaturation due to net heterotrophic conditions.

We primarily focus our analysis in this study on interpretation of spatial patterns in $\Delta O_2/Ar$, since this is determined directly from the dissolved gas measurements. However, we also present calculations of the air-sea flux of biological oxygen driven by this biological saturation anomaly, termed "bioflux" by Jonsson et al. (2013):

$$\text{bioflux} = k \left[O_2 \right]_{eq} \cdot \frac{\Delta O_2}{Ar}$$

where k represents the wind speed-dependent air-sea gas transfer velocity and $[O_2]_{eq}$ is the oxygen concentration that would be expected in the mixed layer were it in equilibrium with the atmosphere. We calculate k using, calculated from daily wind speed data from the NOAA National Climatic Data Center's multiple-satellite Blended Sea Winds product (https://www.ncdc.noaa.gov/data-access/marineocean-data/blended-global/blended-sea-winds) following the Nightingale et al. (2000) equation and the 60-day (Reuer et al., 2007) time-dependent weighting scheme. Mean uncertainty in calculated bioflux is 6.4 ± 3.2 mol O_2 m^{-2} d^{-1}, determined by a Monte Carlo error analysis incorporating cruise-specific O_2/Ar measurement uncertainty and 14% uncertainty in k (as determined by Palevsky, Quay, Lockwood, et al., 2016). In conditions with limited influence of physical advection, entrainment, and transient changes due to non-steady-state conditions over the dissolved gas residence time in the mixed layer, bioflux is equivalent to NCP. However, as noted in Section 1.2, there are potential biases in quantifying bioflux and NCP based on observed $\Delta O_2/Ar$ in dynamic western boundary current regions where steady-state assumptions are likely invalid and strong vertical turbulent dissipation rates have been observed. For this reason, we utilize observed $\Delta O_2/Ar$ as a tracer of biological productivity rather than bioflux.

2.3. Sea Level Anomaly and Mixed Layer Depth Data

To identify the location of the KE front and associated mesoscale eddies, we used $1/4° \times 1/4°$ gridded daily SLA and MDT products that merge data from multiple satellites to obtain a high-resolution view of the dynamics of the upper ocean (the Ssalto/Duacs altimeter products produced and distributed by the Copernicus Marine and Environment Monitoring Service, CMEMS). Closed contours of SLA that enclose a hill/depression of sea level indicate the location of an anti-cyclonic/cyclonic (clockwise/anti-clockwise) eddy. Associated anomalies in thermocline depth mirror the SLA. For each cruise, we determined the date at which the cruise track crossed the KE front and used the SLA data for that day for our analysis of the correlations between $\Delta O_2/Ar$, Chl, and SLA. For May 2011, September 2011, and July 2012 cruises, we used SLA data for the dates of 19/05/2011, 23/09/2011, and 27/07/2012, respectively. We derived the absolute dynamic topography (ADT) for each of these dates by adding the SLA to the MDT, providing streamlines of the geostrophic flow. The container ships collecting the underway data crossed the region of interest within a 4-day to 5-day period and we did not find any large changes in SLA within that time frame. To compare the higher resolution underway data to the satellite data, we binned and averaged the underway data into each of the $1/4° \times 1/4°$ SLA grid cells coinciding with the ship tracks.

We do not have direct estimates of the MLD from the cruises presented here, but to provide some context for the physical environment we have used the MILA GPV mixed layer product, based on the 0.125 kg m^{-3}

criterion, which generates gridded MLD maps from Argo profiles at 10 days intervals (Hosoda et al., 2010). The MILA GPV data were matched up to the cruise dates and used to generate maps and histograms of the MLD over the KE region. MILA GPV data for the following 10-day intervals were used: 19/05/2011–28/05/2011, 22/07/2012–31/07/2012, and 16/09/2011–25/09/2011 for the May 2011, July 2012, and September 2011 cruises, respectively.

2.4. Nitrate and Oxygen Data

Samples for dissolved nutrient analyses were collected from the underway seawater line at roughly the same frequency as the Chl samples, every 6–8 h. These samples were analyzed at the University of Washington Marine Chemistry Laboratory using standard methods (Intergovernmental Oceanography Commission, 1994). Although nutrient samples were collected at the surface concurrently with the $\Delta O_2/Ar$ and Chl data, these data do not provide any information on the vertical structure of the nutrient fields in the KE region. The depth of the nutricline has been shown to vary considerably across the KE front (Clayton et al., 2014; Nagai & Clayton, 2017) and this is likely to be an important control on nutrient availability in the surface mixed layer within the KE region. To understand possible links between nutrient availability, Chl and $\Delta O_2/Ar$, we make use of a range of available, vertically resolved, in situ data collected between 2010 and 2017. This includes data collected by BGC-Argo floats and Japan Meteorological Association (JMA) repeat sections within the KE region in the period before and after our cruises. BGC-Argo nitrate and oxygen data were downloaded directly from the MBARI Chemical Sensor Group's FloatViz page (http://www.mbari.org/science/upper-ocean-systems/chemical-sensor-group/floatviz/), and were comprised of measurements made by two BGC-Argo floats (WMO numbers 5904034 and 5904035), both equipped with nitrate sensors and deployed in the KE region in March 2013. Float 5904034 and float 5904035 continued collecting data until early March 2017 and early January 2017, respectively. Only data from the floats flagged as "good" was used in our analysis. In addition, we used nitrate data from the following JMA cruises: 10-07 (October 2010), 11-08 (July–August 2011), 11-09 (September 2011), 12-03 (April–May 2012), 12-05 (June–July 2012), 12-06 (July–September 2012), 13-04 (April–May 2013), 14-04 (April–May 2014), 15-04 (April–May 2015), and 16-04 (April–May 2016). Data from all of the JMA cruises are publicly available from the JMA data portal (http://www.data.jma.go.jp/gmd/kaiyou/db/vessel_obs/data-report/html/ship/ship_e.php).

During our study period, the KE took a zonal path, and was in its stable mode with no large-scale meander (e.g., Figure 3; Qiu et al., 2014). The nitrate data from the JMA repeat cruises and BGC-Argo floats (listed above) also corresponded to the KE's stable mode, thus allowing us to use that data to construct a composite mean section of the vertical structure of nitrate across the KE region. We excluded data collected during winter months (November, December, January, and February) when the surface nutrient signals can be driven by deep winter mixing (Wong et al., 2002). Finally, we restricted the analysis to the top 150 m of the water column to capture the spatial patterns in nitrate within the surface mixed layer and the top of the nutricline across the KE region.

3. Results and Discussion

3.1. Physical Setting and Observed Distributions of $\Delta O_2/Ar$, Chl, and Nitrate

Each of the three container ship transects crossed the KE front, with the May and September 2011 tracks both crossing the KE front at roughly $145° - 147°E$ (Figures 1a and 2). The July 2012 transect was offset and crossed the KE front closer to the coast of Japan where the Kuroshio deflects and becomes the KE. During the study period (May 2011 to July 2012), the KE front was in its stable mode with a shorter path length, a more northerly path, and relatively fewer mesoscale eddies (Qiu et al., 2014). As a result, we expect that differences between May and September should be driven primarily by seasonality, rather than differences in the level of mesoscale eddy activity. The transect in July transited a region mostly to the north of the KE front, so differences between July and the other two months are likely a combination of seasonal and regional differences.

We obtained concurrent estimates of MLDs based on the 0.125 kg m^{-3} criterion across the KE region from the MILA GPV data product (Figure 3). There was a wide variability in MLDs in May 2011, compared to lower variability in July 2012 and September 2011, with an observed range from 12.5 to 95.9 m and a
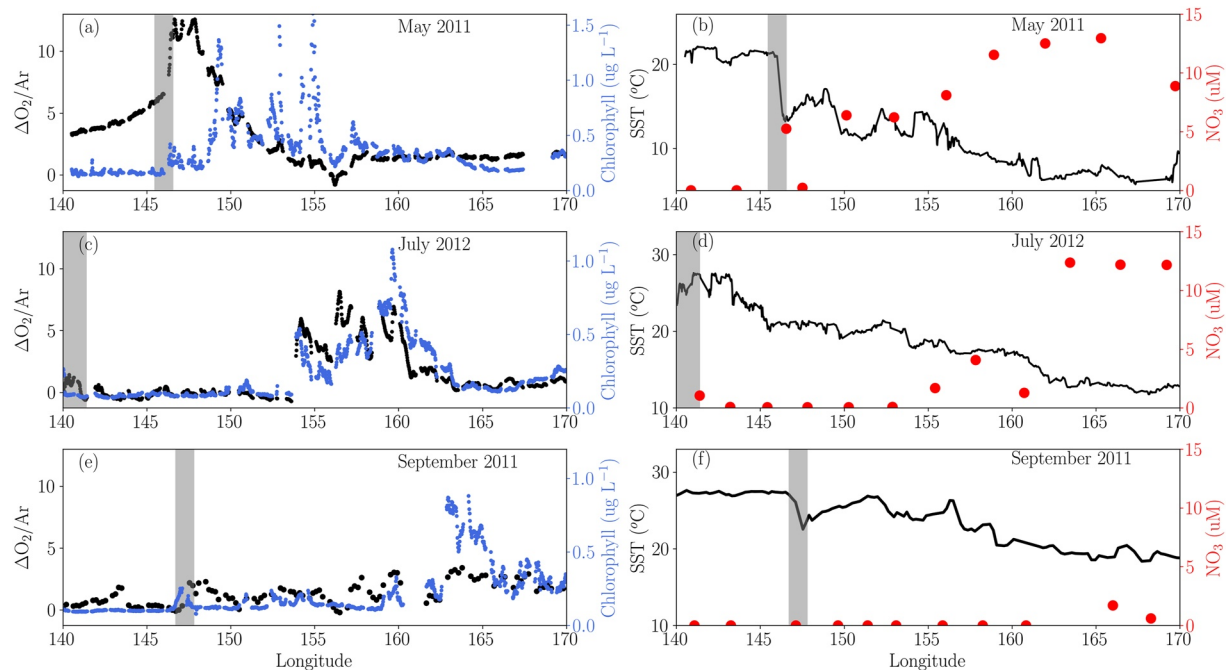
Figure 2. Underway surface physical and biogeochemical properties. The left-hand column shows measurements of $\Delta O_2/Ar$ (black) and Chl derived from calibrated underway fluorescence measurements (blue) for the (a) May 2011, (c) July 2012 and, (e) September 2011 cruises. The right-hand column shows sea surface temperature (SST) from the ship's underway thermosalinograph system (black) and discrete NO_3 measurements (red) for the (b) May 2011, (d) July 2012 and, (f) September 2011 cruises. Note the different scales on the y-axes for Chl and SST. The shaded gray areas on all of the panels show the approximate longitudinal range over which the containership crossed the KE front.

relatively consistent shift to deeper MLDs in the northeastern sector of the KE region. However, the majority of observed MLDs in May were shallower with a median value of 26.5 m and an interquartile range of 25.8 m. In July 2012, the MLD was much less variable across the region with a median value of 14.2 m and interquartile range of 4.4 m. Finally, in September 2011, the median MLD was 24.3 m with an interquartile range of 9.8 m.

Across all three cruises, we find a large-scale gradient in biogeochemical properties related to surface water temperatures. Surface nitrate increases with decreasing surface water temperatures, however, this general pattern is overlaid by sharp localized increases along the shiptracks particularly in May and July (Figure 2, Table 1), which both see large stepwise increases at around 150° and 164°E, respectively. Surface Chl values exhibit much higher variability along track, with marked regions of higher Chl found at roughly 150–155°, 154–162°, and 163–166°E in May, July, and September, respectively. In May, the transition from very low to higher surface nitrate concentrations occurs directly at the KE front, although we do observe some localized variability in nitrate between 145°E and 148°E (Figure 2b). In July surface nitrate concentrations remain low until much further north of the KE front (~160°E), although there is a slight localized increase in surface nitrate concentrations directly at the KE front (~142°E; Figure 2d). There is another localized increase in surface nitrate concentrations in July between 155° and 160°E, which corresponds to a region of high surface Chl. Surface nitrate concentrations are consistently low all along the transect in September (Figure 2f), with a slight increase toward the northeastern extent of the shiptrack at 165–170°E, which coincides with an area of high Chl. Surface $\Delta O_2/Ar$ is consistently low and with relatively low variability along the shiptrack in September, although it does exhibit an increase at and to the north of the KE front, as well as general uptick toward the northeastern extent of the track, east of 160°E.

The highest $\Delta O_2/Ar$ values seen in the July 2012 data are found within a region bounded by ~154° and 165°W (Figures 2c and 4b), spanning roughly 600 km of the cruise track, and coincide with a region of higher nitrate and Chl of comparable extent (Figures 2c and 2d). The Rossby radius of deformation in this region is ~30 km (Chelton et al., 1998), so this high $\Delta O_2/Ar$ feature is far too large scale to be associated with mesoscale eddies. We also note that during the July 2012 cruise there was relatively low eddy activity in the
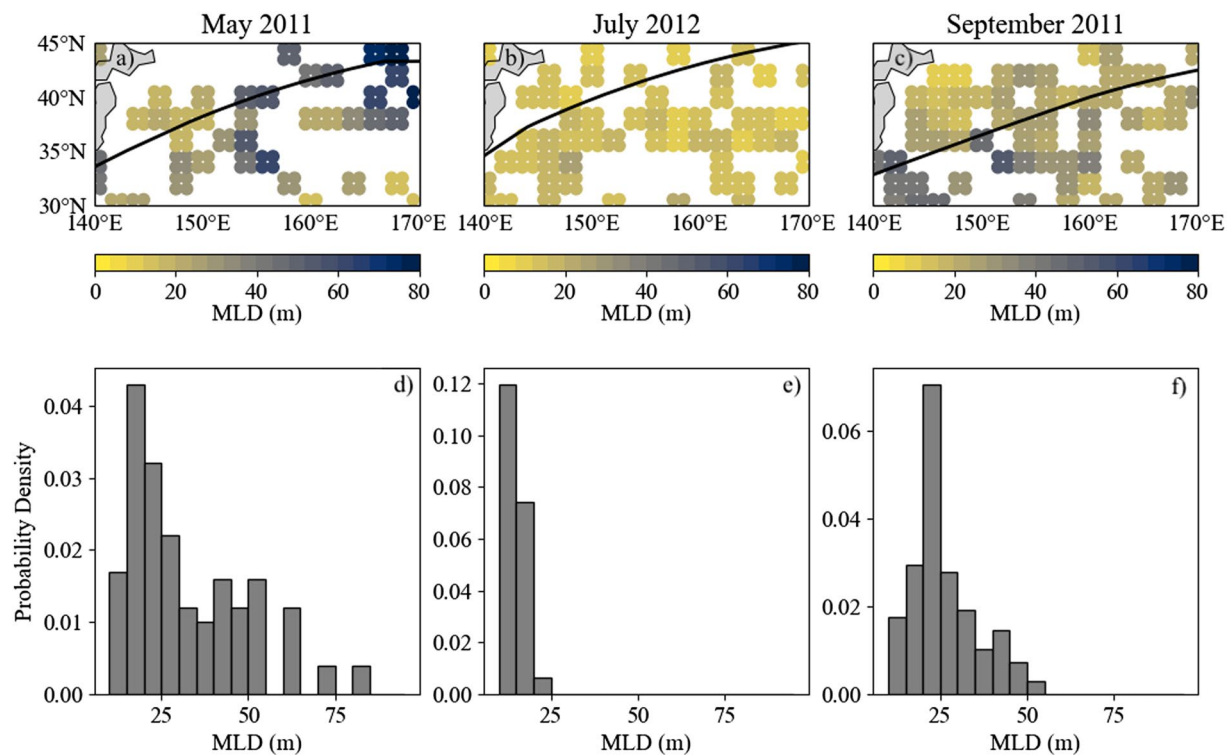
Figure 3. MILA GPV 10-day mixed layer depths for the KE region based on Argo profile data using the 0.125 kg m^{-3} density criterion. The top row shows the spatial extent of the data used and the corresponding ship track overlain as a solid black line for (a) May 2011, (b) July 2012, and (c) September 2011. The second row shows the histograms of observed mixed layer depths (MLDs) for (d) May 2011, (e) July 2012, and (f) September 2011. The histograms are adjusted such that the area under the bars is equal to 1, yielding a probability density function from the data. Note that the MLD scales are the same across panels (a–c) as well as across panels (d–f).

area to the north of the KE front. Although about five coherent mesoscale eddies can be seen to the south of the KE front (Figure 4b), there are no such features to the north. Similarly, during July 2012, the dynamic range of ADT was smaller to the north of the KE front than to the south (Figure 4b). This is all indicative of a region with less eddy activity to the north than to the south of the KE front, and suggests that the high $\Delta O_2/Ar$ observed in the north was related to the large-scale circulation rather than mesoscale activity. To investigate how locations of high $\Delta O_2/Ar$, Chl, and nitrate are associated with the background water masses, we examined variations in T/S space (Figure 5). The water mass associated with the Oyashio Current has a characteristic salinity range of roughly $33.0 < S < 33.5$ (Yamamoto et al., 1988), and $T < 18°C$ (Figure 5a). This water mass also shows elevated values of both nitrate (Figure 5a) and $\Delta O_2/Ar$ (Figure 5b). The eastward flowing Oyashio Current has been shown to bring nutrient-rich coastal waters into the subarctic interior of the North Pacific (Kono & Sato, 2010), with this pathway reflected by the MDT contours that originate near Hokkaido (the northernmost island in Figure 1a).

Table 1
Summary Statistics for $\Delta O_2/Ar$ (%) and Chl ($\mu g\ L^{-1}$) Data

		Mean ± st. dev	Minimum	Maximum
May 2011	$\Delta O_2/Ar$	3.0 ± 2.8	−0.79	12.6
	Chl	0.4 ± 0.2	0.2	1.3
July 2012	$\Delta O_2/Ar$	0.9 ± 2.0	−1.14	8.16
	Chl	0.2 ± 0.2	0.1	1.1
September 2011	$\Delta O_2/Ar$	1.1 ± 1.0	−1.08	3.82
	Chl	0.2 ± 0.2	0.1	0.9

*Note.* The statistics for Chl are based on the calibrated underway fluorescence data.

3.2. Correlations With SLA: Influence of Mesoscale Processes on $\Delta O_2/Ar$ and Chl

The correlation between SLA and $\Delta O_2/Ar$ or Chl gives an indication of the importance of mesoscale features (particularly eddies) in driving the observed distributions of $\Delta O_2/Ar$ and Chl. We examined correlations between SLA and $\Delta O_2/Ar$ for each of the cruises individually (Table 2 and Figure 6). Overall, the highest $\Delta O_2/Ar$ values are associated with low SLA (cyclonic cold-core eddies), however, we did not find a consistent negative relationship between $\Delta O_2/Ar$ and SLA as might be expected if
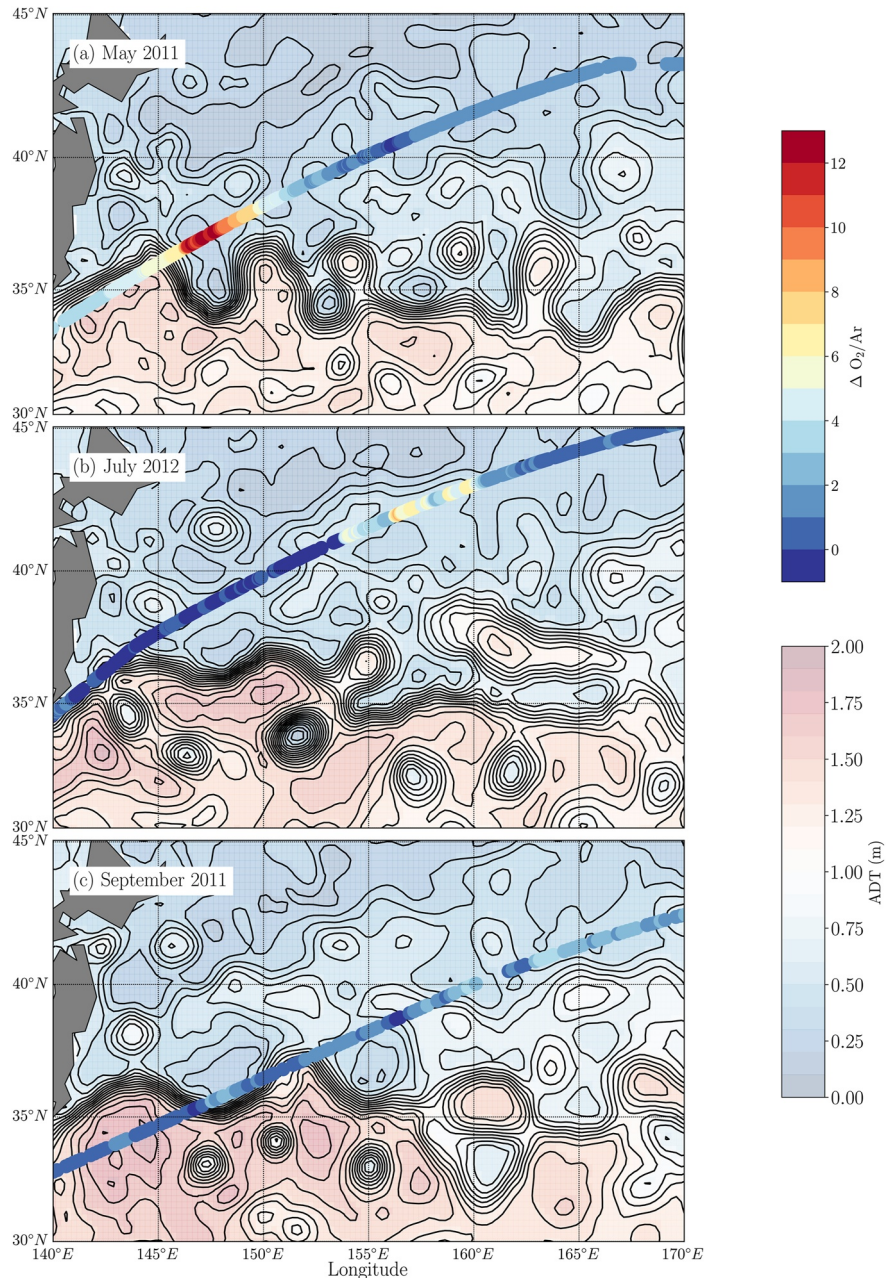
Figure 4. Daily maps of absolute dynamic topography (ADT) with $\Delta O_2/Ar$ overlain for the (a) May 2011, (b) July 2012 and, (c) September 2011 cruises. The ADT is also indicated by black contour lines on each panel. The ADT defines the streamlines of the surface geostrophic flow field. Regions of large spatial gradients in ADT, where contours are closely spaced, indicate regions of large geostrophic current. The Kuroshio can be seen as the region of large gradients in ADT along the coast of Japan, with the Kuroshio Extension taking a zonal path to the East into the North Pacific. The geostrophic currents are directed parallel to lines of constant ADT, with high values of ADT to the right and low values on the left.

biological productivity were consistently suppressed when the thermocline is deepened, or if productivity were enhanced when the thermocline (nutracline) shoals in low nutrient regions. We found no significant relationship between $\Delta O_2/Ar$ and SLA in the May 2011 data when analyzed over the full KE region. However, when the data was split into two subsets from north and south of the KE front, defined by temperatures greater than 18°C to the south and less than 18°C to the north, we found two distinct $\Delta O_2/Ar$ versus SLA regimes. South of the KE front, with SST >18°C, we found a weak positive correlation between $\Delta O_2/Ar$ and
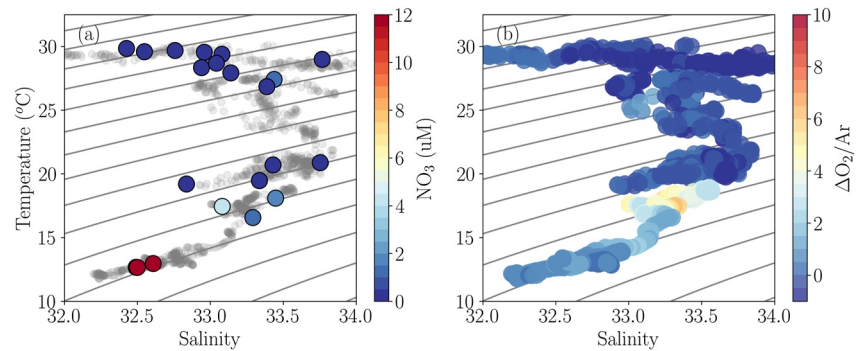
Figure 5. T/S diagrams showing the distribution of (a) surface nitrate concentrations, and (b) $\Delta O_2/Ar$ for the July 2012 cruise. The gray lines show density contours, and the gray circles in panel (a) show the same underway T/S data points as in panel (b).

SLA ($r = 0.23$; Figure 6a). North of the KE front, with SST <18 °C, we found a strong negative correlation between $\Delta O_2/Ar$ and SLA ($r = -0.78$). In the September 2011 data, we also found a moderate negative correlation between $\Delta O_2/Ar$ and SLA ($r = -0.56$) over the entire cruise track, spanning both sides of the KE front (Figure 6c). We also determined the correlation between Chl and SLA (Table 2 and Figure 6). In May 2011, we found a consistent weak negative correlation between Chl and SLA ($r = -0.48$; Figure 6d) across the full cruise track, which is not improved by splitting the data by temperature as was done for $\Delta O_2/Ar$ (Figure 6c). In the September 2011 data, we found a weak positive correlation between Chl and SLA ($r = 0.33$; Figure 6f). For July 2012, when most of the data were collected to the north of the KE front, visual inspection of the data shows that the $\Delta O_2/Ar$ and Chl data do not exhibit a linear correlation, hence our omission of trend lines from Figures 6b and 6e and regression statistics from Table 2.

It is expected that in cyclonic eddies (negative SLA features), the MLD and thermocline should shoal and the nutricline will be brought closer to the surface. These relationships would be expected to drive increased primary production and enhanced Chl concentrations in these eddies in nutrient-limited regions. Indeed, previous studies in the KE region have found negative correlations between SLA and satellite-derived Chl estimates. Kouketsu et al. (2015) found consistently negative correlations between SLA and Chl along, and to the north of, the KE front, but positive correlations between SLA and Chl in the recirculation gyre to the south of the KE front. Although our analysis of the surface Chl data provides results consistent with this previous work, we find a positive correlation between $\Delta O_2/Ar$ and SLA in the warmer waters which form the recirculation gyre to the south of the KE axis in the May 2011 data (Figure 6a) which suggests that deepening of the mixed layer within positive SLA features may act to resupply nutrients into a shallow, nutrient-depleted surface layer, thereby promoting enhanced productivity. Although limited to the available in situ data, these results shown in Figure 6 suggest that the relationships between SLA and Chl, and SLA and $\Delta O_2/Ar$ vary over the year such that mesoscale physical processes can impact Chl and $\Delta O_2/Ar$ in different ways at different times of the year.

3.3. Influence of the Kuroshio Extension and Oyashio Currents on $\Delta O_2/Ar$ and Chl

The highest observed $\Delta O_2/Ar$ values in May 2011 occur where the shiptrack crosses the KE front. Similarly, in July 2012, the highest observed $\Delta O_2/Ar$ values appear to coincide with the Oyashio current. This suggests that large-scale current systems such as a KE and the Oyashio play a role in driving locally enhanced productivity in the region. These currents drive an eastward advection of elevated nutrients which has been observed in the subsurface (Nagai & Clayton, 2017), and whose signature was also observed in the surface nitrate data in this study (Figure 2). Also associated with these currents is the outcropping of isopycnal
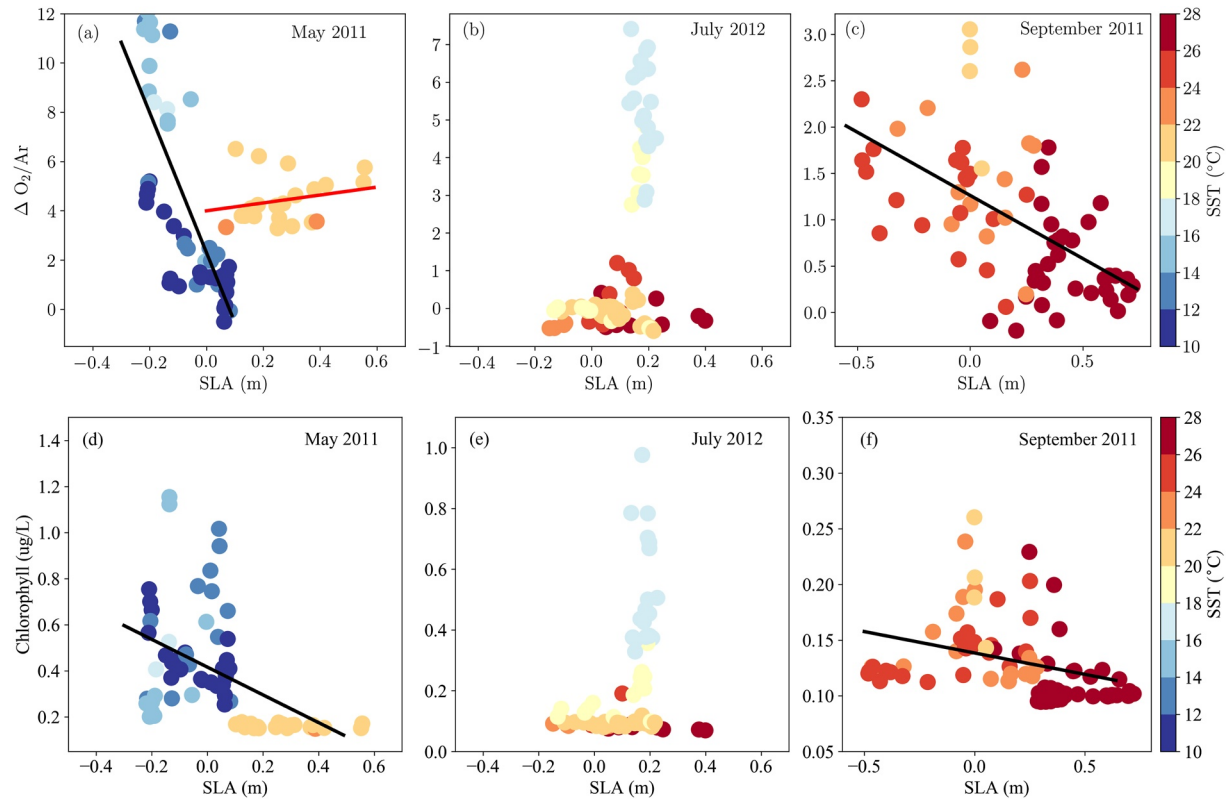
Table 2

Pearson Correlation Coefficients (r-Values) for $\Delta O_2/Ar$ and Chl With Respect to SLA, and Their Respective p-Values for May and September 2011

	Correlation coefficient	*p*-value
May 2011		
$\Delta O_2/Ar$	−0.32	0.38 (not significant)
$\Delta O_2/Ar$ ($T \geq 18°C$)	0.23	<0.05
$\Delta O_2/Ar$ ($T < 18°C$)	−0.78	<0.05
Chl	−0.48	<0.05
September 2011		
$\Delta O_2/Ar$	−0.56	<0.05
Chl	−0.33	<0.05

Note. Nor correlations were found for July 2012.

Figure 6. The relationship between SLA and $\Delta O_2/Ar$ for the (a) May 2011, (b) July 2012 and, (c) September 2011 cruises. Regression lines are plotted on (a) for $T > 18°C$ (red line) and $T < 18°C$ (blue line); and on (c) for all points (black line). The relationship between SLA and Chl for the (d) May 2011, (e) July 2012 and, (f) September 2011 cruises The correlation coefficients and p-values for these data are given in Table 2. Note the different ranges on the y-axes for each of these plots.

layers at the surface, with the potential for the along-isopycnal transport of biogeochemical properties such as nutrients from depth to the surface. Thus the underlying vertical structure of the nitrate distribution is likely to have an impact on surface productivity through a combination of along-isopycnal vertical nutrient supply where isopycnals outcrop, and cross-isopycnal vertical nutrient supply where submesoscale dynamics enhance turbulent dissipation.

We examine the in situ nitrate data from the top 150 m to discern regions or isopycnal ranges where we would expect an enhanced supply of the nitrate to the euphotic zone due to the KE nutrient stream and the outcropping of isopycnals associated with the KE and the Oyashio. While most of the nitrate data were not collected currently with the $\Delta O_2/Ar$ measurements, this additional nitrate data from JMA and BGC-Argo were taken during the same time of the year as the $\Delta O_2/Ar$ data (April–October). We bin the nitrate data in σ_θ versus latitude bins (Figure 7) to provide a common framework for relating the vertical nitrate distribution to surface biogeochemical tracers via σ_θ. In addition, we create a relative isopycnal nitrate anomaly metric, NO3′, which is designed to show how the binned nitrate concentration in any given latitude and σ_θ bin relates to the mean along isopycnal nitrate concentration.

$$NO3'(\text{lat}, \sigma_\theta) = \frac{NO3_{\text{binned}}(\text{lat}, \sigma_\theta)}{NO3_{\text{mean}}(\sigma_\theta)} - 1$$

NO3′ is zero where the binned nitrate concentration is equal to the mean nitrate concentration for that particular isopycnal. Where NO_3' is positive/negative, the binned nitrate concentration is higher/lower than the mean nitrate concentration for that particular isopycnal.

Thus, NO3′ allows an examination of how nitrate varies along isopycnals in the upper 150 m of the water column (Figure 7). Over large scales, surfaces of constant nitrate concentrations tend to be aligned along
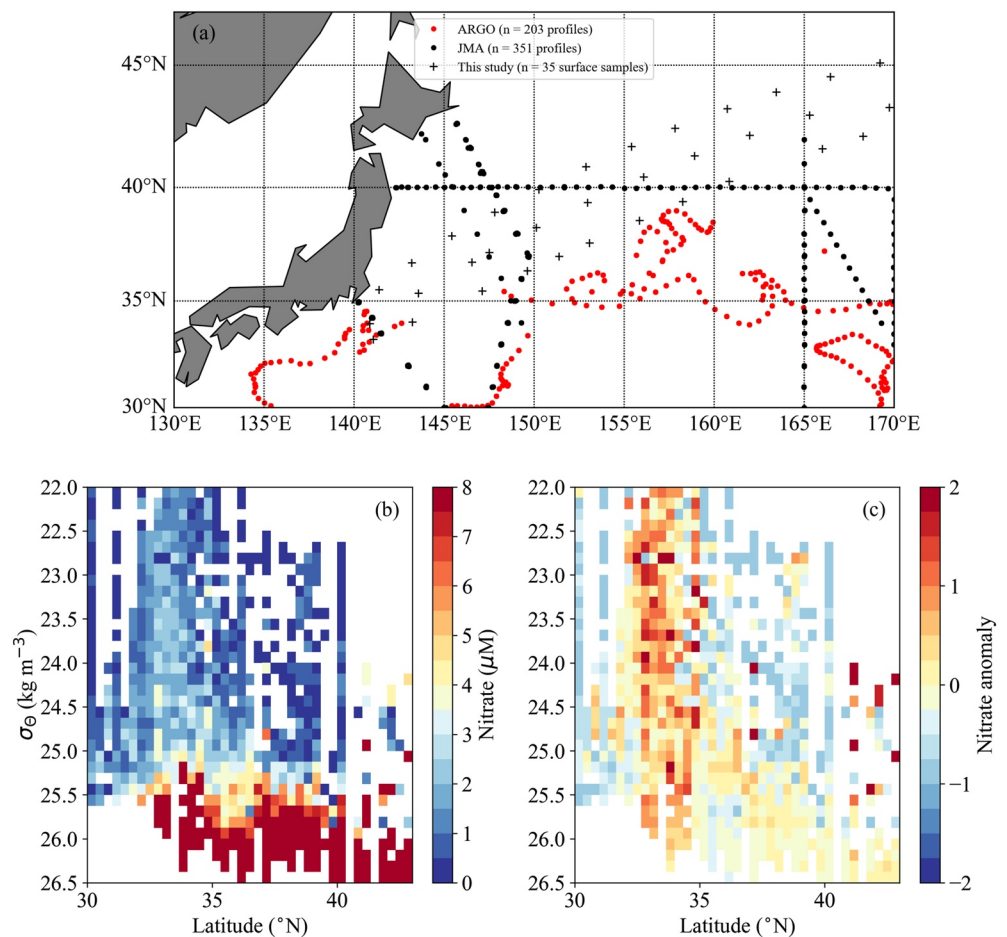
Figure 7. (a) Map of locations of Biogeochemical-Argo (red dots) and JMA (black dots) nitrate depth profiles in the KE region, and locations of surface nitrate samples from the container ship cruises undertaken as part of this study (black crosses), which were used to construct the binned averages in panel (b) and the nitrate anomaly in panel (c). (b) Bin-averaged nitrate data in latitude versus σ_θ space. (c) Relative isopycnal nitrate anomaly (dimensionless) in latitude versus σ_θ space. The data used here was limited to profiles made between April and October from the top 150 m, to limit the influence of higher nutrient values driven by winter mixing. Binning was done using $1/3°$ latitude bins and 0.125 kg m^{-3} σ_θ bins.

isopycnals (Omand & Mahadevan, 2013), however in Figure 7b, we find pronounced along-isopycnal variability in nitrate concentrations. That is, values of the nitrate concentration are not constant along isopycnal surfaces, indicating some local enhancement or reduction in nitrate or localized mixing. In fact, we find a positive nitrate anomaly along isopycnals in the vicinity of the KE front (~35°N, Figure 7c). For a given isopycnal the concentration of nitrate is higher near the KE front than it is away from the front along that same isopycnal. This positive anomaly in nitrate is most apparent between 32.5° and 35.5°N, and between the 22.5 and 25.5 kg m^{-3} isopycnals with respect to waters to the north and south (Figure 7c). For example, the nitrate concentrations along the 24.5 kg m^{-3} isopycnal increase from ~0 µmol/kg at 30°N to 2–3 µmol kg^{-1} at 34°N, then decrease to 0.5–1 µmol kg^{-1} at 36°N and then decrease further to ~0 µmol kg^{-1} at 38°N. This result is consistent with large nitrate anomalies previously observed on the same 24.5 kg m^{-3} isopycnal within a 50 km swath centered on the KE front in a much finer scale survey of the KE front that took place over a period of 5 days (Nagai & Clayton, 2017). Here, we are able to identify the positive nitrate anomaly extending over a wider latitudinal range owing to the larger spatial domain of the available data. Although the data in the northern latitudinal range is sparser, there is also some indication of a positive nitrate anomaly at ~42°N between the 24.0 and 25.5 kg m^{-3} isopycnals which coincide with the density and latitudinal range of the Oyashio Current. It is likely that this is indicative of lateral advection of nutrient-rich waters by the Oyashio (Kono & Sato, 2010). These subsurface nitrate anomalies may drive an enhanced supply of
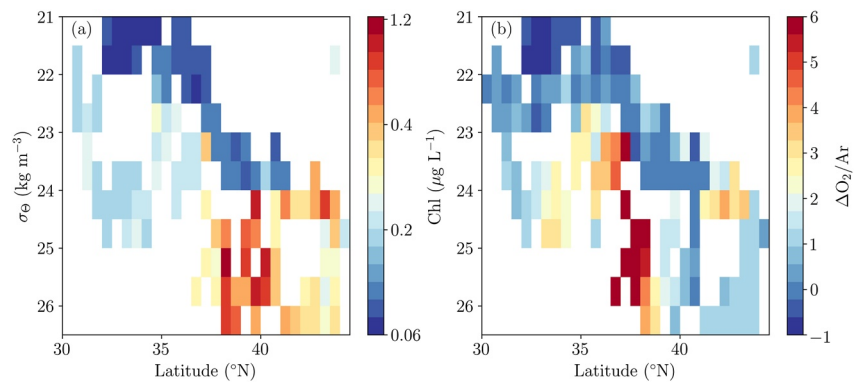
Figure 8. Bin-averaged (a) Chl ($\mu g\ L^{-1}$) from the May, July and September cruises, and (b) $\Delta O_2/Ar$ (%) from the May, July, and September cruises, in latitude versus σ_θ space (note that Chl is shown on a $\log_{10}$ scale). Binning was done using 0.5° latitude bins and 0.5 kg m^{-3} σ_θ bins. We use these larger bin sizes compared to Figure 7 to allow for the smaller number of data points included in the analysis.

nitrate to the surface when those isopycnals outcrop and reach the surface, and this surface nutrient supply would likely be offset in latitude due to the slope of the isopycnals with depth. The signature of the KE nutrient stream, and to a lesser extent an Oyashio nitrate anomaly, suggests that these features in nitrate are consistent and persistent features of the KE region that follow the KE and Oyashio currents as they flow eastward from Japan.

We combine and bin the $\Delta O_2/Ar$ and Chl data in latitudinal and isopycnal bins, as with nitrate (Figure 8), and find that $\Delta O_2/Ar$ and Chl have a somewhat similar distribution, with higher values of both tracers found in the 23.0–26.5 kg m^{-3} isopycnal range, although the high values of $\Delta O_2/Ar$ are largely restricted to two distinct latitudinal bands between 35.5–38.5° and 41–43.5°N, and the higher Chl values tend to be found in at latitudes of 37°N and above. The regions of high $\Delta O_2/Ar$ overlap, but do not correspond exactly, in both latitude and isopycnal space with the nitrate anomalies associated with the KE and the Oyashio currents. The region of high Chl occupies a larger area of the density and latitude space, but does not extend as far south as the higher $\Delta O_2/Ar$ values. Although the regions of high Chl and high $\Delta O_2/Ar$ are offset somewhat in latitude from the marked positive nitrate anomaly spanning 32.5°–35.5°N, they are found in the same isopycnal range (Figure 7). These isopycnal layers outcrop in the broader KE region. Although the $\Delta O_2/Ar$ and Chl data were restricted to surface measurements, the variations of surface density provide a link to the vertical distribution of nitrate and nitrate anomaly along those density surfaces that outcrop (Figure 7).

Isopycnals with elevated $\Delta O_2/Ar$ and positive nitrate anomalies associated with the KE nutrient stream and the Oyashio demonstrate the role of both lateral advection of nutrients by these currents, and localized vertical nutrient supply potentially driven by both along-isopycnal transport and localized cross-isopycnal mixing. However, the Chl data do not quite follow the same pattern as $\Delta O_2/Ar$. Our data, although restricted to three individual cruises agree with the annual climatologies of Chl in this region which show an increase with latitude, suggesting that the data presented here is capturing consistent large-scale regional patterns in Chl. This result supports the hypothesis that $\Delta O_2/Ar$ in the KE region is impacted by nutrients supplied by the large-scale current systems in this region, particularly in spring and summer.

3.4. (De)Coupling Between Chl and $\Delta O_2/Ar$

One of the more striking results of this work is the apparent seasonal and regional shift in the relationship between $\Delta O_2/Ar$ and Chl, and that the relationship of these variables to SLA varies by season. This suggests that Chl is not a consistent tracer for productivity in this region. We see a strong decoupling between $\Delta O_2/Ar$ and Chl in the May 2011 data (Figure 2a), with essentially no correlation ($r = -0.06$; $p < 0.05$) between $\Delta O_2/Ar$ and Chl. In contrast, in the July data, $\Delta O_2/Ar$ and Chl are very strongly correlated ($r = 0.81$; $p < 0.01$; Figure 2c). Similarly, $\Delta O_2/Ar$ and Chl are also strongly positively correlated along the entire shiptrack in the September 2011 data ($r = 0.60$; $p < 0.01$; Figure 2e). Previous studies based on concurrent $\Delta O_2/Ar$ and Chl measurements have also found strong variations in the correlation between either $\Delta O_2/Ar$ or NCP and Chl.
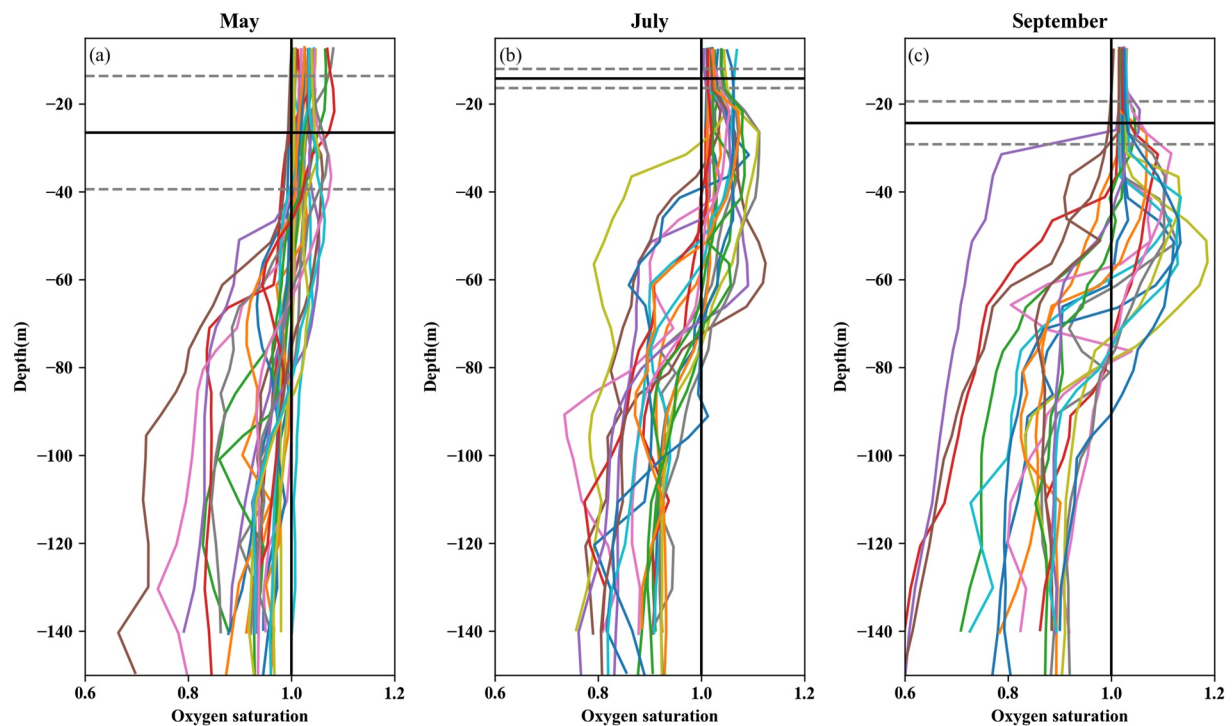
Figure 9. Profiles of O$_2$ saturation from BGC-Argo float data for (a) May, (b) July, and (c) September. The solid black horizontal line shows the median MLD for that month, and the dashed gray horizontal lines bound the interquartile range of MLD for that month. The solid black vertical line at 1 denotes the line where observed O$_2$ is equal to the O$_2$ saturation concentration for the local temperature and salinity conditions.

In high latitude systems, strong correlations between NCP and Chl are observed during the spring bloom (Tortell & Long, 2009), in summer (Tortell et al., 2012), and across a springtime productivity hotspot at the transition between the coastal and open ocean (Palevsky et al., 2013), but much weaker correlations after the peak of a bloom (Tortell et al., 2011). Conversely, a study in the equatorial Pacific found no correlation at all between NCP and Chl (Stanley et al., 2010). Previous studies have also demonstrated spatial decoupling between NCP and export of particles from the mixed layer (Estapa et al., 2015), as well as 2–15 days temporal lags between peaks in surface Chl concentrations and in export flux (Stange et al., 2017). Our results expand on these previous studies by showing how the correlations between ΔO$_2$/Ar and Chl vary in a given region across more than one season.

Here, we outline some potential mechanisms to explain the observed decoupling between ΔO$_2$/Ar and Chl. The May 2011 ΔO$_2$/Ar data indicates a large excess of O$_2$ relative to Ar in the surface mixed layer to the north of the KE front. In steady-state conditions, such as an excess of O$_2$ can either be attributed to net autotrophy (production of O$_2$ through photosynthesis exceeding removal through respiration), or a physical flux of O$_2$ into the mixed layer, most commonly due to vertical mixing. We first examine the possibility that the excess O$_2$ is due to mixing of high O$_2$ waters from below the base of the mixed layer. Although we do not have concurrent O$_2$ profiles for these cruises, we examine the O$_2$ profiles from the BGC-Argo floats used in the nitrate analysis (Figure 9). In May, profiles of O$_2$ saturation are relatively uniform and consistently oversaturated within the surface mixed layer and tend to become undersaturated deeper into the water column. If these data can be expected to be representative of the conditions within the study region, we could expect that the high ΔO$_2$/Ar signal observed in May is most likely due to in situ net productivity rather than a physical transport of high O$_2$ into the surface mixed layer from below. In contrast, the data show a stronger tendency for an increase in O$_2$ saturation below the mixed layer in July and August (Figures 9b and 9c), with the strongest signal observed in September.

Absent significant physical supply of water supersaturated in oxygen, elevated ΔO$_2$/Ar indicates net photosynthetic production. In steady-state conditions, high ΔO$_2$/Ar driven by elevated NCP but without an associated increase in Chl would require an ecosystem where the majority of organic carbon produced is quickly

exported from the mixed layer rather than accumulating biomass in the surface. However, bloom conditions create a deviation from steady state, such that the high $\Delta O_2/Ar$ in the region north of the KE axis in May 2011 could reflect an early- phase bloom feature driven by increasing NCP that has produced high $\Delta O_2/Ar$ but where biomass has not yet had sufficient time to accumulate and produce high Chl concentrations. Similarly, the region farther east on the May 2011 transect with low $\Delta O_2/Ar$ but high Chl concentrations could either reflect a senescent bloom phase, where biomass remains high but NCP has diminished due to a rise in respiration or decrease in primary production. Although remote sensing data could be used to provide temporal context, albeit at coarser spatial resolution, extensive cloud cover prevented clear views of the region in May 2011, limiting our ability to explore the temporal context of those data.

Finally, the observed decoupling could also be due to differences in the integration times of $\Delta O_2/Ar$ and Chl. The KE front is a strongly advective system, with horizontal current speeds O (1 m s^{-1}), which could result in a decoupling between instantaneously measured properties such as Chl, and O_2/Ar gas ratios which by their nature give an integrated view over the water parcel's trajectory that is dependent on the dissolved gas residence time (Teeter et al., 2018). Previous work has estimated a 3 days lag between nutrient injection events (based on the meandering dynamics of the front) and the appearance of high Chl patches downstream along a trajectory (Yamazaki et al., 2009), which is shorter than the 5–15 days dissolved gas residence time for the May 2011 transect. Consequently, a combination of strong lateral advection and lags in biological responses likely play an important role in driving some of the observed decoupling between Chl and $\Delta O_2/Ar$, and should be considered when interpreting data collected from similar regions.

Our study provides synoptic high spatial-resolution observations across the KE region, with each cruise providing a snapshot view of the system. This has the advantage that we can capture spatial/regionally variability, but the disadvantage of this approach is that we cannot resolve transient temporal contexts (e.g., bloom stage) that might influence the observed relationships between $\Delta O_2/Ar$ and Chl. Future efforts to disentangle potential explanations for both coupled and decoupled relationships between $\Delta O_2/Ar$ and Chl would benefit from temporally as well as spatially resolved measurements of the mixed layer, as well as measurements of export below the mixed layer, and of particulate organic carbon and phytoplankton community composition, since large cells that sink more quickly out of the mixed layer may be more likely to contribute to export than to surface biomass accumulation.

4. Conclusions

In this study, we have investigated the spatial variability of biological productivity in the dynamically active KE region based on the distribution of the productivity tracer $\Delta O_2/Ar$ measured with high resolution synoptic in situ underway data collected during spring, summer, and early fall. These observations reveal large spatial variability in $\Delta O_2/Ar$ and productivity in the KE region at all scales down to the mesoscale and finer. We also find strong correlations between $\Delta O_2/Ar$ and SLA (a proxy for mesoscale eddies), but the sign of these correlations varies seasonally and regionally. Several common threads emerge from our analysis. The KE front is a hotspot of biological productivity within the larger KE region, particularly in spring, with high $\Delta O_2/Ar$ associated with the same density and latitude range as the KE nutrient stream. Similarly, high $\Delta O_2/Ar$ is also associated with the Oyashio Current in the summer time. These observations reveal the extent of fine-scale synoptic variability in $\Delta O_2/Ar$ within the larger KE region. This spatial and temporal variability is lost in large-scale climatological studies, where the KE region is subsumed within broader regional averaging. Resolving and understanding the drivers of this variability is likely to be key in building a mechanistic understanding of the range of factors controlling rates of biological productivity in the region, which ultimately will enable better parameterizations of these processes in Earth System Models.

Our observations also highlight seasonal and regional (de)coupling between $\Delta O_2/Ar$ and Chl which may impact the accuracy of Chl-based estimates of productivity. Previous comparison of geochemical NCP estimates and satellite algorithm-based NCP in the North Pacific has shown that no single algorithm is applicable both in the subarctic and subtropical gyres (Palevsky, Quay, & Nicholson, 2016), confounding the ability to use these algorithms to evaluate NCP across the KE frontal region. Understanding the mechanisms that control the degree of coupling between Chl and $\Delta O_2/Ar$ (and by proxy NCP) will allow us not only to better

understand the processes controlling the biological carbon pump, but also to better predict primary and export productivity from observations of Chl and ocean color.

Although the results of this work suggest several avenues for further study, all require the development of methods for collecting sustained, high-resolution biogeochemical measurements within such dynamic western boundary current regions (Todd et al., 2019). Underway measurements collected from ships of opportunity provide a means of collecting data from repeat lines at high spatial resolution but are restricted to surface waters. To develop a mechanistic understanding of the physical and biological factors controlling $\Delta O_2/Ar$, it is key to observe not only the surface ocean, but also the vertical structure of the mixed layer, the photic zone, and the nutricline. The development and expansion of the Biogeochemical-Argo program (Claustre et al., 2020; Johnson et al., 2009) will be a key source of synoptic data on the vertical biogeochemical structure of the ocean. Here, we have used available BGC-Argo data to put our surface-only observations into context, but the conclusions we can draw are limited by the fact that these data were not collected concurrently. This study, however, highlights the power of combining data collected from a range of observing platforms across different spatial and temporal ranges to build a fuller picture of such a dynamic open ocean system. Future studies combining underway biogeochemical measurements from the ocean surface (e.g., ships of opportunity and saildrones) with vertically resolved data derived from a range of platforms (e.g., floats and gliders) will drive developments in our mechanistic understanding of how biogeochemical processes in dynamic ocean regions are modulated by physical and biological controls.

Data Availability Statement

All of the container ship transect data used in this study are available from the Biological & Chemical Oceanography Data Management Office (http://www.bco-dmo.org/project/626077). Additional data used in this study have been archived in the ODU Digital Commons (https://digitalcommons.odu.edu/oeas_fac_pubs/420/). The altimeter products were produced by Ssalto/Duacs and distributed by Aviso, with support from CNES (http://www.aviso.altimetry.fr/duacs/).

References

Bach, L. T., Stange, P., Taucher, J., Achterberg, E. P., Algueró-Muñiz, M., Horn, H., et al. (2019). The influence of plankton community structure on sinking velocity and remineralization rate of marine aggregates. *Global Biogeochemical Cycles*, *33*(8), 971–994. https://doi.org/10.1029/2019gb006256

Buesseler, K. O., Boyd, P. W., Black, E. E., & Siegel, D. A. (2020). Metrics that matter for assessing the ocean biological carbon pump. *Proceedings of the National Academy of Sciences of the United States of America*, *117*(18), 9679–9687. https://doi.org/10.1073/pnas.1918114117

Carr, M.-E., Friedrichs, M. A. M., Schmeltz, M., Noguchi Aita, M., Antoine, D., Arrigo, K. R., et al. (2006). A comparison of global estimates of marine primary production from ocean color. *Deep-Sea Research, Part I*, *53*, 741–770. https://doi.org/10.1016/j.dsr2.2006.01.028

Cassar, N., Barnett, B. A., Bender, M. L., Kaiser, J., Hamme, R. C., & Tilbrook, B. (2009). Continuous high-frequency dissolved O_2/Ar measurements by equilibrator inlet mass spectrometry. *Analytical Chemistry*, *81*(5), 1855–1864. https://doi.org/10.1021/ac802300u

Castro-Morales, K., Cassar, N., Shoosmith, D. R., & Kaiser, J. (2013). Biological production in the Bellingshausen Sea from oxygen-to-argon ratios and oxygen triple isotopes. *Biogeosciences*, *10*(4), 2273–2291. https://doi.org/10.5194/bg-10-2273-2013

Chelton, D. B., DeSzoeke, R. A., Schlax, M. G., El Naggar, K., & Siwertz, N. (1998). Geographical variability of the first baroclinic Rossby radius of deformation. *Journal of Physical Oceanography*, *28*(3), 433–460. https://doi.org/10.1175/1520-0485(1998)028<0433:gvotfb>2.0.co;2

Claustre, H., Johnson, K. S., & Takeshita, Y. (2020). Observing the global ocean with biogeochemical-argo. *Annual Review of Marine Science*, *12*, 23–48. https://doi.org/10.1146/annurev-marine-010419-010956

Clayton, S., Nagai, T., & Follows, M. J. (2014). Fine scale phytoplankton community structure across the Kuroshio Front. *Journal of Plankton Research*, *36*(4), 1017–1030. https://doi.org/10.1093/plankt/fbu020

Craig, H., & Hayward, T. (2011). Oxygen supersaturation in the ocean: Biological versus physical contributions. *Science*, *235*(4785), 199–202. https://doi.org/10.1126/science.235.4785.199

D'Asaro, E., Lee, C., Rainville, L., Harcourt, R., & Thomas, L. (2011). Enhanced turbulence and energy dissipation at ocean fronts. *Science*, *332*(6027), 318–322. https://doi.org/10.1126/science.1201515

DeVries, T., Primeau, F., & Deutsch, C. (2012). The sequestration efficiency of the biological pump. *Geophysical Research Letters*, *39*, L13601. https://doi.org/10.1029/2012GL051963

Ducklow, H. W., Steinberg, D. K., & Buesseler, K. O. (2001). Upper ocean carbon export and the biological pump. *Oceanography*, *14*(4), 50–58. https://doi.org/10.5670/oceanog.2001.06

Emerson, S., Quay, P., Stump, C., Wilbur, D., & Knox, M. (1991). O_2, Ar, N_2 and 222Rn in surface waters of the subarctic ocean: Net biological O_2 production. *Global Biogeochemical Cycles*, *5*(1), 49–69. https://doi.org/10.1029/90gb02656

Estapa, M. L., Siegel, D. A., Buesseler, K. O., Stanley, R. H. R., Lomas, M. W., & Nelson, N. B. (2015). Decoupling of net community and export production in the Sargasso Sea. *Global Biogeochemical Cycles*, *29*. https://doi.org/10.1002/2013GB004579

Eveleth, R., Cassar, N., Sherrell, R. M., Ducklow, H., Meredith, M. P., Venables, H. J., et al. (2017). Ice melt influence on summertime net community production along the Western Antarctic Peninsula. *Deep-Sea Research Part II Topical Studies in Oceanography*, *139*, 89–102. https://doi.org/10.1016/j.dsr2.2016.07.016

Garcia, H. E., & Gordon, L. I. (1992). Oxygen solubility in seawater: Better fitting solubility equations. *Limnology and Oceanography*, *37*(6), 1307–1312. https://doi.org/10.4319/lo.1992.37.6.1307

Giering, S. L., & Humphreys, M. P. (2018). *Biological pump* (pp. 1–6). Springer International Publishing. https://doi.org/10.1007/978-3-319-39193-9_154-1

Guo, X. Y., Zhu, X. H., Long, Y., & Huang, D. J. (2013). Spatial variations in the Kuroshio nutrient transport from the East China Sea to south of Japan. *Biogeosciences*, *10*(10), 6403–6417. https://doi.org/10.5194/bg-10-6403-2013

Guo, X. Y., Zhu, X. H., Wu, Q., & Huang, D. J. (2012). The Kuroshio nutrient stream and its temporal variation in the East China Sea. *Journal of Geophysical Research: Oceans*, *117*(C1). https://doi.org/10.1029/2011jc007292

Hamme, R. C., Cassar, N., Lance, V. P., Vaillancourt, R. D., Bender, M. L., Strutton, P. G., et al. (2012). Dissolved O_2/Ar and other methods reveal rapid changes in productivity during a Lagrangian experiment in the Southern Ocean. *Journal of Geophysical Research: Oceans*, *117*(C4). https://doi.org/10.1029/2011jc007046

Hamme, R. C., & Emerson, S. (2004). The solubility of neon, nitrogen and argon in distilled water and seawater. *Deep-Sea Research, Part I*, *51*(11), 1517–1528. https://doi.org/10.1016/j.dsr.2004.06.009

Haskell, W., Fassbender, A., Long, J., & Plant, J. (2020). Annual net community production of particulate and dissolved organic carbon from a decade of biogeochemical profiling float observations in the Northeast Pacific. *Global Biogeochemical Cycles*, *34*(10), e2020GB006599. https://doi.org/10.1029/2020gb006599

Haskell, W. Z., & Fleming, J. C. (2018). Concurrent estimates of carbon export reveal physical biases in ΔO_2/Ar-based net community production estimates in the Southern California Bight. *Journal of Marine Systems*, *183*, 23–31. https://doi.org/10.1016/j.jmarsys.2018.03.008

Henson, S. A., Beaulieu, C., & Lampitt, R. (2016). Observing climate change trends in ocean biogeochemistry: When and where. *Global Change Biology*, *22*(4), 1561–1571. https://doi.org/10.1111/gcb.13152

Honda, M. C., Sasai, Y., Siswanto, E., Kuwano-Yoshida, A., Aiki, H., & Cronin, M. F. (2018). Impact of cyclonic eddies and typhoons on biogeochemistry in the oligotrophic ocean based on biogeochemical/physical/meteorological time-series at station KEO. *Progress in Earth and Planetary Science*, *5*(1). https://doi.org/10.1186/s40645-018-0196-3

Honda, M. C., Wakita, M., Matsumoto, K., Fujiki, T., Siswanto, E., Sasaoka, K., et al. (2017). Comparison of carbon cycle between the western Pacific subarctic and subtropical time-series stations: Highlights of the K2S1 project. *Journal of Oceanography*, *73*, 647–667. https://doi.org/10.1007/s10872-017-0423-3

Hosoda, S., Ohira, T., Sato, K., & Suga, T. (2010). Improved description of global mixed-layer depth using Argo profiling floats. *Journal of Oceanography*, *66*(6), 773–787. https://doi.org/10.1007/s10872-010-0063-3

Imai, K., Nojiri, Y., Tsurushima, N., & Saino, T. (2002). Time series of seasonal variation of primary productivity at station KNOT (44 oN, 155 oE) in the sub-arctic western North Pacific. *Deep-Sea Research, Part II*, *49*, 5395–5408. https://doi.org/10.1016/s0967-0645(02)00198-4

Intergovernmental Oceanography Commission. (1994). *Protocols for the Joint Global Ocean Flux Study (JGOFS) core measurements*. UNESCO.

Izett, R. W., Manning, C. C., Hamme, R. C., & Tortell, P. D. (2018). Refined estimates of net community production in the subarctic Northeast Pacific derived from ΔO_2/Ar measurements with N_2O-based corrections for vertical mixing. *Global Biogeochemical Cycles*, *32*(3), 326–350. https://doi.org/10.1002/2017gb005792

Johnson, K., Berelson, W., Boss, E., Chase, Z., Claustre, H., Emerson, S., et al. (2009). Observing biogeochemical cycles at global scales with profiling floats and gliders: Prospects for a global array. *Oceanography*, *22*(3), 216–225. https://doi.org/10.5670/oceanog.2009.81

Jonsson, B. F., Doney, S. C., Dunne, J., & Bender, M. (2013). Evaluation of the Southern Ocean O_2/Ar-based NCP estimates in a model framework. *Journal of Geophysical Research: Biogeosciences*, *118*(2), 385–399. https://doi.org/10.1002/jgrg.20032

Kaiser, J., Reuer, M. K., Barnett, B., & Bender, M. L. (2005). Marine productivity estimates from continuous O_2/Ar ratio measurements by membrane inlet mass spectrometry. *Geophysical Research Letters*, *32*(19). https://doi.org/10.1029/2005GL023459

Kaneko, H., Yasuda, I., Komatsu, K., & Itoh, S. (2013). Observations of vertical turbulent nitrate flux across the Kuroshio. *Geophysical Research Letters*, *40*(12), 3123–3127. https://doi.org/10.1002/grl.50613

Kono, T., & Sato, M. (2010). A mixing analysis of surface water in the Oyashio region: Its implications and application to variations of the spring bloom. *Deep Sea Research Part II: Topical Studies in Oceanography*, *57*(17–18), 1595–1607. https://doi.org/10.1016/j.dsr2.2010.03.004

Kouketsu, S., Kaneko, H., Okunishi, T., Sasaoka, K., Itoh, S., Inoue, R., & Ueno, H. (2015). Mesoscale eddy effects on temporal variability of surface chlorophyll a in the Kuroshio Extension. *Journal of Oceanography*, *72*(3), 439–451. https://doi.org/10.1007/s10872-015-0286-4

Lockwood, D., Quay, P. D., Kavanaugh, M. T., Juranek, L. W., & Feely, R. A. (2012). High-resolution estimates of net community production and air-sea CO_2 flux in the northeast Pacific. *Global Biogeochemical Cycles*, *26*(4). https://doi.org/10.1029/2012gb004380

Mackas, D. L., Denman, K. L., & Abbott, M. R. (1985). Plankton patchiness – Biology in the physical vernacular. *Bulletin of Marine Science*, *37*(2), 652–674.

Mahadevan, A. (2015). The impact of submesoscale physics on primary productivity of plankton. *Annual Review of Marine Science*, *8*, 161–184. https://doi.org/10.1146/annurev-marine-010814-015912

Manning, C. C., Howard, E. M., Nicholson, D. P., Ji, B. Y., Sandwith, Z. O., & Stanley, R. H. R. (2017). Revising estimates of aquatic gross oxygen production by the triple oxygen isotope method to incorporate the local isotopic composition of water. *Geophysical Research Letters*, *44*, 1–10. https://doi.org/10.1002/2017GL074375

Martin, A. P., & Srokosz, M. A. (2002). Plankton distribution spectra: Inter-size class variability and the relative slopes for phytoplankton and zooplankton. *Geophysical Research Letters*, *29*(24), 66. https://doi.org/10.1029/2002gl015117

Matsumoto, K., Abe, O., Fujiki, T., Sukigara, C., & Mino, Y. (2016). Primary productivity at the time-series stations in the northwestern Pacific Ocean: Is the subtropical station unproductive? *Journal of Oceanography*, *72*(3), 359–371. https://doi.org/10.1007/s10872-016-0354-4

McGillicuddy, D. J., Jr. (2016). Mechanisms of physical-biological-biogeochemical interaction at the oceanic mesoscale. *Annual Review of Marine Science*, *8*, 125–159. https://doi.org/10.1146/annurev-marine-010814-015606

Nagai, T., & Clayton, S. (2017). Nutrient interleaving below the mixed layer of the Kuroshio Extension Front. *Ocean Dynamics*, *67*, 1027–1046. https://doi.org/10.1007/s10236-017-1070-3

Nagai, T., Tandon, A., Yamazaki, H., & Doubell, M. J. (2009). Evidence of enhanced turbulent dissipation in the frontogenetic Kuroshio Front thermocline. *Geophysical Research Letters*, *36*(12). https://doi.org/10.1029/2009gl038832

Nagai, T., Tandon, A., Yamazaki, H., Doubell, M. J., & Gallager, S. (2012). Direct observations of microscale turbulence and thermohaline structure in the Kuroshio Front. *Journal of Geophysical Research*, *117*. https://doi.org/10.1029/2011jc007228

Nightingale, P. D., Malin, G., Law, C. S., Watson, A. J., Liss, P. S., Liddicoat, M. I., et al. (2000). In situ evaluation of air-sea gas exchange parameterizations using novel conservative and volatile tracers. *Global Biogeochemical Cycles*, *14*(1), 373–387. https://doi.org/10.1029/1999gb900091

Omand, M. M., & Mahadevan, A. (2013). Large-scale alignment of oceanic nitrate and density. *Journal of Geophysical Research: Oceans*, *118*(10), 5322–5332. https://doi.org/10.1002/jgrc.20379

Palevsky, H. I., Quay, P. D., Lockwood, D. E., & Nicholson, D. P. (2016). The annual cycle of gross primary production, net community production, and export efficiency across the North Pacific Ocean. *Global Biogeochemical Cycles*, *30*(2), 361–380. https://doi.org/10.1002/2015gb005318

Palevsky, H. I., Quay, P. D., & Nicholson, D. P. (2016). Discrepant estimates of primary and export production from satellite algorithms, a biogeochemical model, and geochemical tracer measurements in the North Pacific Ocean. *Geophysical Research Letters*, *43*(16), 8645–8653. https://doi.org/10.1002/2016gl070226

Palevsky, H. I., Ribalet, F., Swalwell, J. E., Cosca, C. E., Cokelet, E. D., Feely, R. A., et al. (2013). The influence of net community production and phytoplankton community structure on CO_2 uptake in the Gulf of Alaska. *Global Biogeochemical Cycles*, *27*(3), 664–676. https://doi.org/10.1002/gbc.20058

Qiu, B., Chen, S., Schneider, N., & Taguchi, B. (2014). A coupled decadal prediction of the dynamic state of the Kuroshio extension system. *Journal of Climate*, *27*(4), 1751–1764. https://doi.org/10.1175/jcli-d-13-00318.1

Racault, M.-F., Le Quéré, C., Buitenhuis, E., Sathyendranath, S., & Platt, T. (2012). Phytoplankton phenology in the global ocean. *Ecological Indicators*, *14*(1), 152–163. https://doi.org/10.1016/j.ecolind.2011.07.010

Ramachandran, S., Tandon, A., & Mahadevan, A. (2014). Enhancement in vertical fluxes at a front by mesoscale-submesoscale coupling. *Journal of Geophysical Research: Oceans*, *119*(12), 8495–8511. https://doi.org/10.1002/2014jc010211

Reuer, M. K., Barnett, B. A., Bender, M. L., Falkowski, P. G., & Hendricks, M. B. (2007). New estimates of Southern Ocean biological production rates from O_2/Ar ratios and the triple isotope composition of O2. *Deep-Sea Research, Part I*, *54*, 951–974. https://doi.org/10.1016/j.dsr.2007.02.007

Ribalet, F., Swalwell, J., Clayton, S., Jimenez, V., Sudek, S., Lin, Y., et al. (2015). Light-driven synchrony of Prochlorococcus growth and mortality in the subtropical Pacific gyre. *Proceedings of the National Academy of Sciences of the United States of America*, *112*(26), 8008–8012. https://doi.org/10.1073/pnas.1424279112

Rosengard, S. Z., Izett, R. W., Burt, W. J., Schuback, N., & Tortell, P. D. (2020). Decoupling of ΔO_2/Ar and particulate organic carbon dynamics in nearshore surface ocean waters. *Biogeosciences*, *17*(12), 3277–3298. https://doi.org/10.5194/bg-17-3277-2020

Stange, P., Bach, L. T., Le Moigne, F. A. C., Taucher, J., Boxhammer, T., & Riebesell, U. (2017). Quantifying the time lag between organic matter production and export in the surface ocean: Implications for estimates of export efficiency. *Geophysical Research Letters*, *44*(1), 268–276. https://doi.org/10.1002/2016GL070875

Stanley, R. H. R., Kirkpatrick, J. B., Cassar, N., Barnett, B. A., & Bender, M. L. (2010). Net community production and gross primary production rates in the western equatorial Pacific. *Global Biogeochemical Cycles*, *24*(4). https://doi.org/10.1029/2009gb003651

Strickland, J. D. H., & Parsons, T. R. (1972). *A practical handbook of seawater analysis* (2nd ed.). Fisheries Research Board of Canada Bulletin.

Teeter, L., Hamme, R. C., Ianson, D., & Bianucci, L. (2018). Accurate estimation of net community production from O_2/Ar measurements. *Global Biogeochemical Cycles*. *32*(8), 1163–1181. https://doi.org/10.1029/2017gb005874

Todd, R. E., Chavez, F. P., Clayton, S., Cravatte, S., Goes, M., Graco, M., et al. (2019). Global perspectives on observing ocean boundary current systems. *Frontiers in Marine Science*, *6*. https://doi.org/10.3389/fmars.2019.00423

Tortell, P. D. (2005). OCEANOGRAPHY: Methods dissolved gas measurements in oceanic waters made by membrane inlet mass spectrometry. *Most*, *2*, 24–37. https://doi.org/10.4319/lom.2005.3.24

Tortell, P. D., Bittig, H. C., Körtzinger, A., Jones, E. M., & Hoppema, M. (2015). Biological and physical controls on N_2, O_2, and CO_2 distributions in contrasting Southern Ocean surface waters. *Global Biogeochemical Cycles*, *29*, 994–1013. https://doi.org/10.1002/2014GB004975

Tortell, P. D., Guéguen, C., Long, M. C., Payne, C. D., Lee, P., & DiTullio, G. R. (2011). Spatial variability and temporal dynamics of surface water pCO₂, ΔO_2/Ar and dimethylsulfide in the Ross Sea, Antarctica. *Deep Sea Research Part I: Oceanographic Research Papers*, *58*(3), 241–259. https://doi.org/10.1016/j.dsr.2010.12.006

Tortell, P. D., & Long, M. C. (2009). Spatial and temporal variability of biogenic gases during the Southern Ocean spring bloom. *Geophysical Research Letters*, *36*(1). https://doi.org/10.1029/2008gl035819

Tortell, P. D., Long, M. C., Payne, C. D., Alderkamp, A.-C., Dutrieux, P., & Arrigo, K. R. (2012). Spatial distribution of pCO₂, ΔO_2/Ar and dimethylsulfide (DMS) in polynya waters and the sea ice zone of the Amundsen Sea, Antarctica. *Deep Sea Research Part II: Topical Studies in Oceanography*, *71–76*, 77–93. https://doi.org/10.1016/j.dsr2.2012.03.010

Ulfsbo, A., Cassar, N., Korhonen, M., Heuven, S. V., Hoppema, M., Kattner, G., & Anderson, L. G. (2014). Late summer net community production in the central Arctic Ocean using multiple approaches Adam. *Global Biogeochemical Cycles*, *28*, 1129–1148. https://doi.org/10.1002/2014GB004833

van Gennip, S., Martin, A. P., Srokosz, M. A., Allen, J. T., Pidcock, R., Painter, S. C., & Stinchcombe, M. C. (2016). Plankton patchiness investigated using simultaneous nitrate and chlorophyll observations. *Journal of Geophysical Research: Oceans*, *121*, 4149–4156. https://doi.org/10.1002/2016jc011789

Volk, T., & Hoffert, M. I. (1985). Ocean carbon pumps: Analysis of relative strengths and efficiencies in ocean-driven atmospheric CO_2 changes. *The Carbon Cycle and Atmospheric CO_2: Natural Variations Archean to Present*, *32*, 99–110.

Wakita, M., Honda, M. C., Matsumoto, K., Fujiki, T., Kawakami, H., Yasunaka, S., et al. (2016). Biological organic carbon export estimated from the annual carbon budget observed in the surface waters of the western subarctic and subtropical North Pacific Ocean from 2004 to 2013. *Journal of Oceanography*, *72*(5), 665–685. https://doi.org/10.1007/s10872-016-0379-8

Wang, S., Kranz, S. A., Kelly, T. B., Song, H., Stukel, M. R., & Cassar, N. (2020). Lagrangian studies of net community production: The effect of diel and multiday nonsteady state factors and vertical fluxes on O_2/Ar in a dynamic upwelling region. *Journal of Geophysical Research: Biogeosciences*, *125*(6). https://doi.org/10.1029/2019jg005569

Wong, C. S., Waser, N. A. D., Nojiri, Y., Whitney, F. A., Page, J. S., & Zeng, J. (2002). Seasonal cycles of nutrients and dissolved inorganic carbon at high and mid latitudes in the North Pacific Ocean during the Skaugran cruises: Determination of new production and nutrient uptake ratios. *Deep-Sea Research, Part II*, *49*, 5317–5338. https://doi.org/10.1016/s0967-0645(02)00193-5

Yamamoto, T., Nishizawa, S., & Taniguchi, A. (1988). Formation and retention of phytoplankton peak abundance in the Kuroshio Front. *Journal of Plankton Research*, *10*(6), 1113–1130. https://doi.org/10.1093/plankt/10.6.1113

Yamazaki, H., Iwamatsu, I., Hasegawa, D., & Nagai, T. (2009). Chlorophyll patches observed during summer in the main stream of the Kuroshio. *Atmosphere-Ocean*, *47*(4), 299–307. https://doi.org/10.3137/oc306.2009